Topological crystalline insulator (Pb,Sn)Te: Surface states and their spin polarization

S. Safaei, P. Kacman, and R. Buczko*

Institute of Physics, Polish Academy of Sciences, Aleja Lotników 32/46, 02-668 Warsaw, Poland

(Received 28 March 2013; published 8 July 2013)

Using a tight-binding approach we study theoretically the nature of surface states in $Pb_{0.4}Sn_{0.6}Te$—the recently discovered topological crystalline insulator. Apart from the (001) surface states previously studied, two other surface families, {011} and {111}, in which the mirror symmetry of the crystal's rocksalt structure plays the same role in topological protection, are considered. Our calculations show that while in (111) surface states of (Pb,Sn)Te four single, topologically protected Dirac cones should appear, for the (110) surface states the protection is lifted for two L points. In this case, instead of the Dirac points energy gaps occur in the surface states, due to the interaction between the two L valleys. In all studied cases a chiral spin texture is obtained.

DOI: 10.1103/PhysRevB.88.045305 PACS number(s): 71.20.−b, 71.70.Ej, 73.20.At, 79.60.−i

I. INTRODUCTION

In recent years the study of topological phenomena has become one of the major topics of condensed-matter physics.[1,2] This was initiated by the theoretical prediction[3–5] and the succeeding experimental discovery[6–8] of topological insulators (TIs). In TIs the bulk insulating states are accompanied by metallic helical Dirac-like electronic states on the surface of the crystal. In this class of materials spin-orbit coupling and time-reversal symmetry combine to form topologically protected states and feature a chiral spin texture, thus providing robust spin-polarized conduction channels. In the search for TIs, primarily narrow-gap semiconductors, in which the band gaps are smaller than relativistic corrections to the band structure, have been considered. The TI phase was first demonstrated in two dimensions, i.e., in HgTe/HgCdTe quantum wells[6] and also in InAs/GaSb heterostructures.[9] Examples of three-dimensional TI phases include Bi_2Se_3 and Bi_2Te_3 (Refs. 1 and 2) with an odd number of band inversions, which support gapless Dirac-like surface states. The narrow-gap IV-VI semiconductors PbTe, PbSe, and SnTe, as well as their substitutional solid solutions, $Pb_{1-x}Sn_xTe$ and $Pb_{1-x}Sn_xSe$, have also been considered, but they were identified as trivial insulators,[4] because in these the band inversion happens simultaneously at an even number (four) of L points in the Brillouin zone. It has been suggested that applying uniaxial strain[4] or exploiting the anisotropic energy quantization of electrons confined at a PbTe/(Pb,Sn)Te interface[10] can be used to solve this problem. Next, Fu introduced the notion of "topological crystalline insulators"[11] (TCIs) and predicted that in a given class of materials the gapless surface states are supported by crystalline symmetry. It has been proposed lately that this TCI phase should exist in SnTe.[12] Soon after it was confirmed by angle-resolved photoelectron spectroscopy studies that indeed metallic surface states exist on the (001) surfaces of SnTe.[13] They have been observed also on the (001) surfaces of the IV-VI substitutional solid solutions $Pb_{1-x}Sn_xSe$ (Ref. 14) and $Pb_{1-x}Sn_xTe$.[15] It has been shown[16] that the compositional disorder in these alloys does not destroy the TCI phase. Very recently, the observation of chiral spin textures of the metallic (001) surface states in the TCI phase of $Pb_{0.73}Sn_{0.27}Se$ (Ref. 17) as well as of $Pb_{0.6}Sn_{0.4}Te$ (Ref. 15) has been reported by spin-resolved photoelectron spectroscopy (SRPES). It should be emphasized that the metallic surface states observed in real SnTe- or SnSe-based compounds have almost linear, Dirac-like dispersions,[12–15] due to the spin-orbit interactions.

In this article we present a systematic theoretical study of the electronic structure, in particular the nature of surface states, in $Pb_{0.4}Sn_{0.6}Te$. The Sn content $x = 0.6$ assures band inversion and the TCI phase in the $Pb_{1-x}Sn_xTe$ material. In this rocksalt TCI surface states with nontrivial Dirac-like energy spectrum can form at various surfaces of the crystal. Each Dirac point, if it appears, corresponds to one of the four L points in the three-dimensional bulk Brillouin zone (3DBZ). As shown in Ref. 12, these Dirac points are topologically protected only at crystal surfaces symmetric about any of the {110} mirror planes (the Dirac points must be situated at the line of such plane symmetry). These are $\{n\ n\ m\}$ surfaces. We study thus, apart from the previously studied (001)-oriented surface, the surface states for the (110) and (111) planes. In Fig. 1 the 3DBZs are appropriately oriented to show the projections onto the (001), (110), and (111) surfaces. The corresponding {110} mirror planes are marked in yellow. As one can see in Fig. 1, while for the (001)-oriented surface there are two such {110} mirror planes, for the (110) surface there is only one and for the (111)-oriented surface there are three such planes. We note that in all three cases the projections of all but one high-symmetry L point of the 3DBZ are situated at the edges of the corresponding two-dimensional Brillouin zones (2DBZs), marked in green in the figure. The one exception is the L_1 point in the (111)-oriented 3DBZ, which projects to the $\overline{\Gamma}$ point in the center of the 2DBZ. We note also that while the 2DBZ for the (111) surface is a regular hexagon, for the two other cases the 2DBZs are rectangular. It can be observed that a hexagonal 2DBZ occurs always when the $\{n\ n\ m\}$ surface indices are all odd numbers. The rectangular shape of the 2DBZ requires different parities of n and m.

The spin polarization of metallic surface states of $Pb_{0.4}Sn_{0.6}Te$ is studied by calculating the spin texture of the surface states. Because the crystal is in the TCI phase, chiral spin texture of the states at all the considered surfaces, (001), (110), and (111), is anticipated. Recently, similar results were presented,[18,19] in which the description of the (001) and (111) surface states by a $k \cdot p$ Hamiltonian was also proposed.

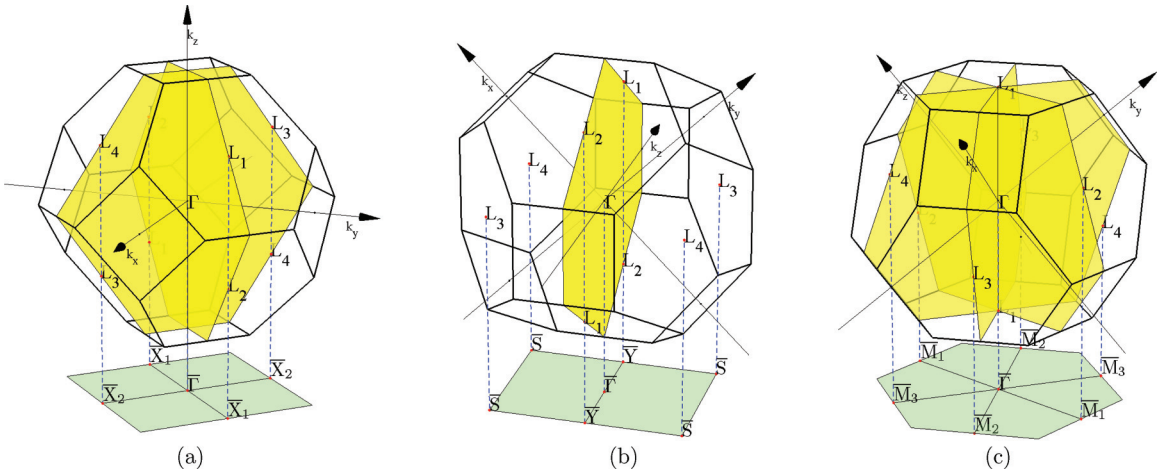

FIG. 1. (Color online) The Brillouin zone for the (a) (001)-, (b) (110)-, and (c) (111)-oriented rocksalt crystal with the corresponding 2DBZs (in green). The {110} mirror planes of the (001) (a), (110) (b), or (c) (111) surface are marked in yellow. In the 2DBZs the {110} mirror plane symmetry lines are also depicted.

II. BAND-STRUCTURE CALCULATIONS

As mentioned above, successive substitution of Pb by Sn in PbTe strongly changes the relativistic effects and results in a compositional evolution of the band structure of the $Pb_{1-x}Sn_xTe$ solid solution. At $x \simeq 0.37$ a band inversion between the topmost valence band and the lowest conduction band occurs, leading to a topological phase transition from a trivial insulator to a TCI state. For higher Sn contents, in the inverted-band-gap state, the formation of Dirac-like surface states that cross the band gap is expected. To study these effects for different surfaces, we consider an alloy well above the critical composition, i.e., $Pb_{0.4}Sn_{0.6}Te$. The electronic surface states in the substitutional alloy $Pb_{0.4}Sn_{0.6}Te$ were obtained by using the tight-binding approach and virtual-crystal approximation. The parameters for the constituent compounds PbTe and SnTe are needed to describe $Pb_{0.4}Sn_{0.6}Te$ within the virtual-crystal approximation. The tight-binding parameters for both PbTe and SnTe were taken from Ref. 20, where they were obtained within a nearest-neighbor 18-orbital sp^3d^5 model. Therefore, in our tight-binding Hamiltonian for $Pb_{0.4}Sn_{0.6}Te$, the s, p, and d orbitals and nearest-neighbor interactions are included. Such a procedure has proved to provide proper dependence of the band gap of the solid solution PbSnTe on the Sn content.[14] In all calculations we use slab geometry with periodic boundary conditions imposed in the two directions parallel to the slab surfaces.

All considered $Pb_{0.4}Sn_{0.6}Te$ solid solution crystal slabs have rocksalt crystal structure, typical for their component IV-VI compounds. For the (001)- and (110)-oriented slabs, the surface states do not depend on the number of atomic monolayers (in particular on the parity of this number), provided the slab is thick enough to separate the surfaces. The results presented here for the (110) surface are obtained on a 315-monolayer-thick slab. The results presented previously in Ref. 14 for the (001) surface states in $Pb_{0.4}Sn_{0.6}Te$ were obtained by the same method on a slab with 280 monolayers. For these two orientations the slabs are always symmetric as the surfaces on both sides of these slabs are identical, independent of the parity of the number of atomic layers. The (111)-oriented slabs are symmetric only when the number of atomic layers is odd. Two symmetric (111)-oriented slabs, each consisting of 451 atomic monolayers, one cation and the other anion terminated, have been used in the calculations of the (111) surface states. This odd number of atomic monolayers enables us to study separately the surfaces consisting of either cations or anions. It should be noted that despite having different numbers of monolayers the thickness of the slabs is similar for all three orientations and is between 70 and 90 nm. This results from different interlayer distances along these directions.

Figure 2 shows the calculated band structure of a (001)-oriented $Pb_{0.4}Sn_{0.6}Te$ slab. The $k = 0$ value corresponds to the projection of the L_3 and L_4 points in the bulk crystal [compare

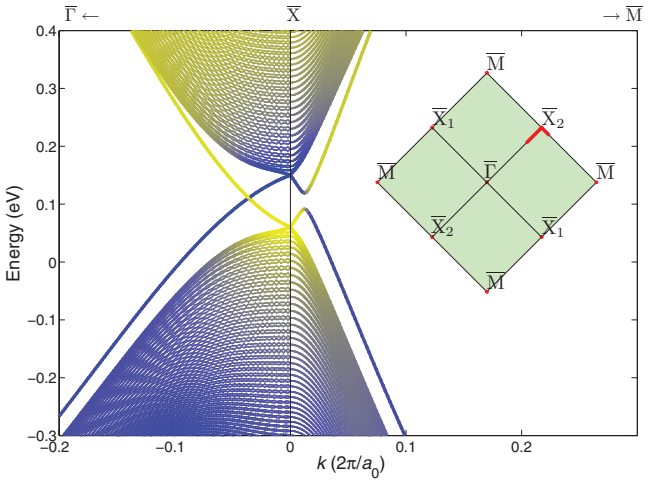

FIG. 2. (Color online) The calculated band structure of a 280-monolayer-thick (001)-oriented $Pb_{0.4}Sn_{0.6}Te$ slab. The line color changes from yellow to blue depending on whether the cation (yellow) or anion (blue) p-type orbitals give the dominant contribution to the wave function. The green rectangle in the inset is the (001) 2DBZ. The energies are calculated for the k values shown in red in the inset.

Fig. 1(a)] onto the (001) surface, i.e., to the $\overline{X}$ point of the surface Brillouin zone. In the figure the wave vector of the electrons, k, is given in units of $2\pi/a_0$, where a_0 is the rocksalt lattice parameter. The energies are calculated for k values in the vicinity of the $\overline{X}$ point of the 2DBZ, along $\overline{\Gamma}$-$\overline{X}$-$\overline{M}$, shown by the red line in the inset. The lowest and highest states of the conduction and valence bands, respectively, represent states localized at the surface. For this surface our calculations confirm the findings reported previously—analogously to the situation in SnTe (Ref. 12) and $Pb_{1-x}Sn_xSe$,[14,17] the (001) surface states for $Pb_{0.4}Sn_{0.6}Te$ are also found to cross the ca. 100 meV inverted bulk band gap along the $\overline{\Gamma}$-$\overline{X}$ direction, i.e., they form a Dirac cone. Around all four $\overline{X}$ points presented in the inset, which are pairwise equivalent, the band structure is of course the same as presented in Fig. 2. Due to the interaction between the L valleys, the four Dirac points are not situated at the two $\overline{X}$ points, but are moved along the projections of the {110} mirror planes, i.e., along the $\overline{\Gamma}$-$\overline{X}$ lines.

In Fig. 3 the calculated band structure of a (110)-oriented $Pb_{0.4}Sn_{0.6}Te$ crystal for the k wave vectors along $\overline{\Gamma}$-$\overline{Y}$-$\overline{S}$-$\overline{\Gamma}$ is presented. In Fig. 3(b) the results of a more precise calculation performed on a thicker slab in the vicinity of the $\overline{Y}$ and $\overline{S}$ points are shown. One can see that around the $\overline{Y}$ point the band structure is similar to that for the (001) surface around the $\overline{X}$ point and surface-state crossing in the band gap is observed. We note that the L points projected to $\overline{Y}$ are the L_1 and L_2 high-symmetry points of the 3DBZ, as presented in Fig. 1(b). As one can see, these two L points are situated on the $(\bar{1}10)$ mirror plane of the (110) surface (marked in yellow in the figure) and thus one can expect the corresponding Dirac points to be topologically protected. At the $\overline{S}$ point of the 2DBZ, however, the protection of the (110) surface states is lifted, because L_3 and L_4, which are projected onto the $\overline{S}$ point, are not situated in the $(\bar{1}10)$ mirror plane, as shown in Fig. 1(b). In the latter case, due to the interaction between the two L valleys, instead of Dirac points energy gaps occur in the surface states along the $\overline{S}$-$\overline{\Gamma}$ lines.

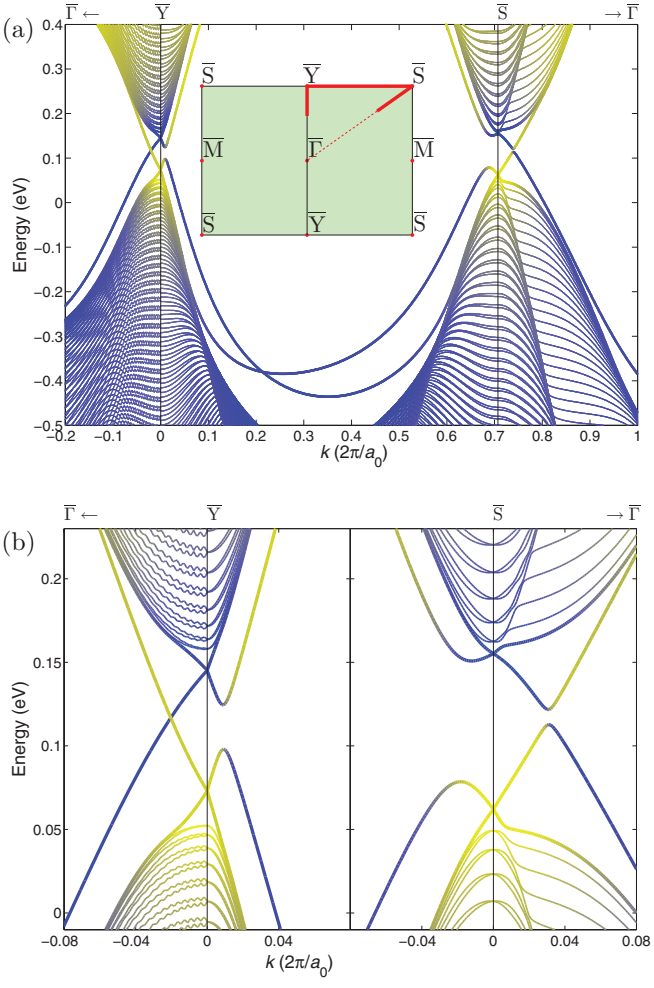

FIG. 3. (Color online) (a) The calculated band structure of a (110)-oriented $Pb_{0.4}Sn_{0.6}Te$ slab, 315 monolayers thick, for the k wave vectors shown in the inset by the red line. The zoomed view (b) of the band structure in the vicinity of the $\overline{Y}$ and $\overline{S}$ points of the 2DBZ was obtained for a thicker $Pb_{0.4}Sn_{0.6}Te$ slab (365 monolayers).

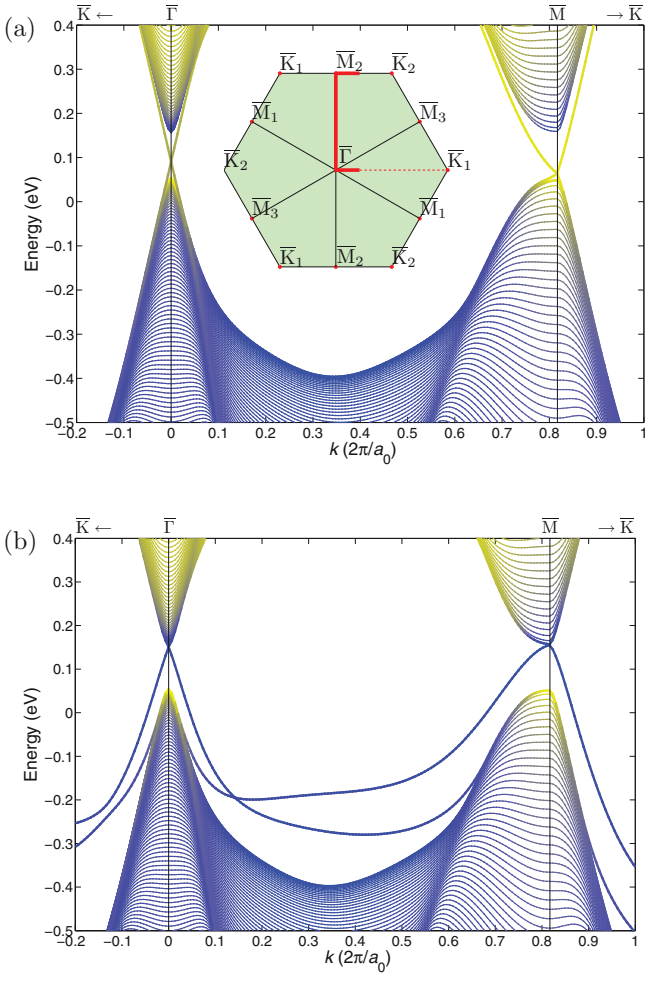

FIG. 4. (Color online) The calculated band structure of a 451-monolayer-thick (111)-oriented $Pb_{0.4}Sn_{0.6}Te$ slab for the k wave vectors of the 2DBZ along $\overline{K}$-$\overline{\Gamma}$-$\overline{M}$-$\overline{K}$, as shown in the inset by the red line. The band structure of the slab with cations at the surfaces is presented in (a), and that with anion surfaces in (b). The blue to yellow color coding indicates again the contributions of the cation (yellow) and anion (blue) p orbitals to the wave functions.

For the last considered surface family, {111}, two cases have to be distinguished, because in this direction the crystal has surfaces composed exclusively of either cations or anions. For both these situations four single, topologically protected Dirac cones (one at the $\overline{\Gamma}$ point and three at the $\overline{M}$ points) are obtained in the calculations. For the anion-terminated slab the bands are brought into contact, forming anion Dirac cones, while in the other case the bands meet to form cation Dirac cones. In Fig. 4 the band structure along the $\overline{K}$-$\overline{\Gamma}$-$\overline{M}$-$\overline{K}$ line, with one pair of Dirac cones, is presented for surfaces consisting of cations (a) and anions (b). For (111) cation surface states the Dirac points appear in the energy gap close to the top of the valence band [see Fig. 4(a)]. For the anion surface states [Fig. 4(b)] the Dirac points are situated just below the conduction band. It should be emphasized that here, in contrast to the situation described above for the (001) and (110) surfaces, all the Dirac points are well separated and appear exactly at the appropriate projection points of the single L points. Moreover, as shown in Fig. 1(c), for the (111) surface all L points belong to the three {110} mirror planes of the (111) surface and, thus, all Dirac points should be topologically protected. We should note, however, that in our study the polarity of the cation- and anion-terminated surfaces is not taken into account. The extra confinement related to the charges on the surfaces can lead to additional Rashba splittings, as shown, for example, for Bi_2Se_3 by Bahramy *et al.*[21]

III. SPIN TEXTURE OF THE SURFACE STATES

As it is well known, at the high-symmetry L points of the studied material the electronic states are eigenstates not of the spin but of the total angular momentum projection operator $j_z = \pm 1/2$. Thus, the surface states in the vicinity of the L-point projections are not eigenstates of the spin. They are composed mostly of the p orbitals and the spin. Still, these nondegenerate surface states are spin polarized. Here we calculate only the expectation values of the spin components, because only they are observed in the SRPES experiments. In the following by "spin" we mean a vector defined by these expectation values. The calculated spin textures for the states above and below the Dirac points are presented in Fig. 5. These spin-polarized states have a chiral spin texture for all three (001), (110), and (111) orientations of the surfaces. For energies above the Dirac points of the (001)-oriented surface, for wave vectors k between the Dirac points (inner vortex) the spin rotates counterclockwise about $\overline{X}$. Outside this region (outer vortex) the rotation is reversed (clockwise). In the local environment of each Dirac point a small left-handed chiral structure is obtained, as predicted in Ref. 12 and observed in the case of $Pb_{0.6}Sn_{0.4}Te$.[15] For energies below the Dirac point all the chiralities are reversed as compared to those obtained for the band above the Dirac point. The clockwise (counterclockwise) chirality is related to the cation (anion) p-type orbitals. This spin texture leads to the conclusion that the mirror Chern number of PbSnTe is equal to -2.[12,19]

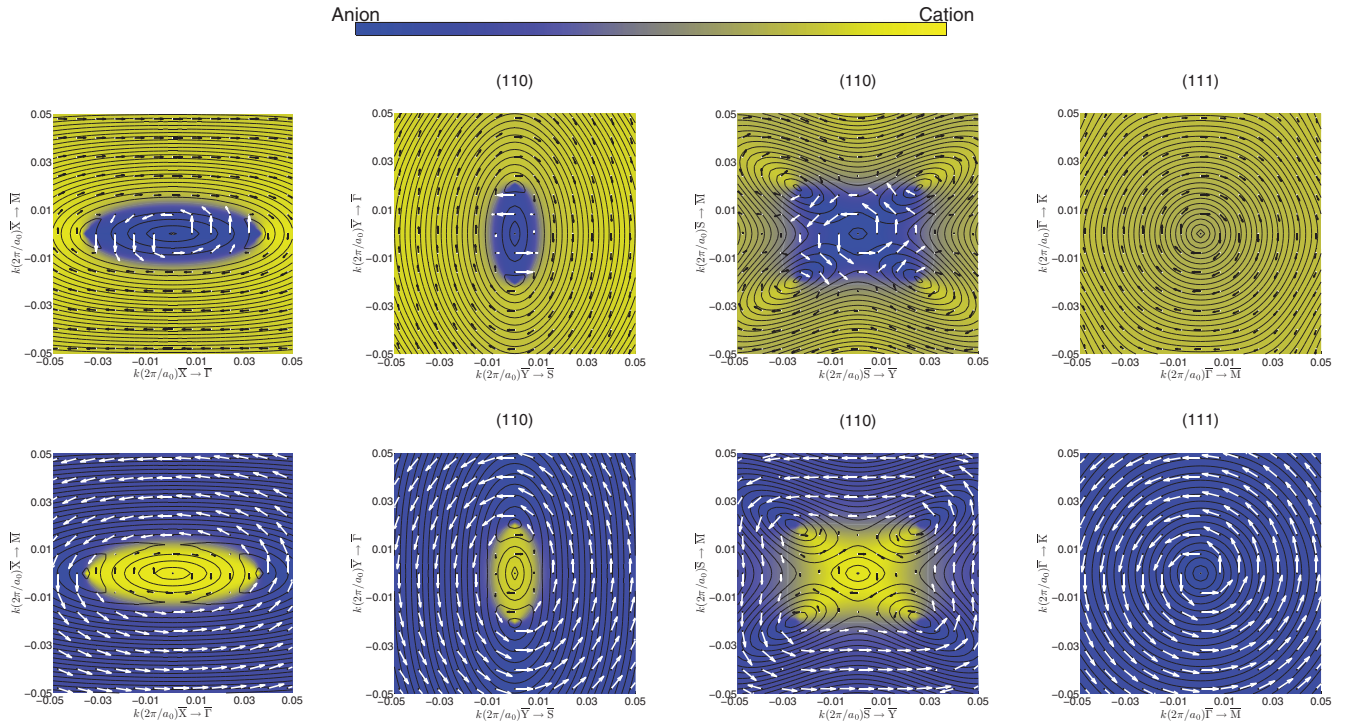

FIG. 5. (Color online) Contour plots of the constant-energy lines of the (001), (110), and (111) surface states of $Pb_{0.4}Sn_{0.6}Te$ above (upper row) and below (lower row) the Dirac point. For the (001) surface the plots are around the $\overline{X}$ point of the 2DBZ, for (110) around two, $\overline{Y}$ (left) and $\overline{S}$ (right), points and for (111) in the vicinity of $\overline{\Gamma}$. For the (111)-oriented surface, in the upper panel the result obtained for the cation-terminated slab is shown, while the lower panel shows the result for the anion-terminated slab. The arrows represent the vectors of the expectation values of in-plane spin components. The arrows' length shows the degree of spin polarization. The blue to yellow color coding indicates again the contributions of the cation (yellow) and anion (blue) p orbitals to the wave functions, as shown by the bar.

For the (110) surface states the spin pattern around the $\overline{Y}$ projection point has also a multivortical structure, similar to that for (001) surface states around the $\overline{X}$ point. Again, the rotation in the outer vortex is opposite to that in the inner vortex. Although a multivortical structure is also obtained for (110) surface states around the $\overline{S}$ projection, the spin texture in this case looks much more complicated. Here, instead of two local vortices around the Dirac points, four local vortices along the $\overline{S}$-$\overline{\Gamma}$ lines are obtained. These local vortices are related to the four energy gaps in the surface states.

For the (111) anion surface states the spin texture is presented only below the Dirac point, because above the Dirac point the surface states are degenerate with the conduction band. Similarly, the cation surface states below the Dirac point enter the valence band. In Fig. 5 we present, therefore, contour plots for the cation surface states only above the Dirac point. Both these plots have the form of single vortices. The spins in the anion (cation) Dirac lower (upper) cones are rotating in opposite directions. We note that these chiralities are the same as those predicted in Ref. 22 and observed in the 3D TIs Bi_2Se_3 and Bi_2Te_3.[8] The same chirality was also predicted in the case of the PbTe/(Pb,Sn)Te (111) interface.[10]

Finally, for the (001) surface it has been shown[12,19] that, by symmetry, the perpendicular to the surface spin component is equal to zero in the whole Brillouin zone. We have checked that this is also the case for the (110) surface, where the same symmetry reasons are valid. Thus, in our spin texture calculations for both (001) and (110) surfaces a zero out-of-plane component of the spin has been obtained. In contrast, for the (111) surface the symmetry requires that the spin component normal to the surface equals zero only along the three high-symmetry $\overline{\Gamma}$-$\overline{M}$ lines. While in the vicinity of the $\overline{\Gamma}$ point, where these lines intersect, the normal spin component vanishes, in the Dirac cones around the $\overline{M}$ points (crossed by only one such line) the out-of-surface spin component appears. The same different behavior of the out-of-(111)-surface spin component at the $\overline{\Gamma}$ and $\overline{M}$ points has been also predicted for the PbTe/(Pb,Sn)Te interface.[10] Moreover, the symmetry requires opposite signs of the components of the spin parallel to the mirror plane for a given k vector and its mirror reflection. Thus, on the mirror symmetry lines [$\overline{\Gamma}$-$\overline{X}$ for the (001) surface, $\overline{\Gamma}$-$\overline{Y}$ and $\overline{Y}$-$\overline{S}$ for the (110) surface, and $\overline{\Gamma}$-$\overline{M}$ for the (111) surface] the spins are perpendicular to the appropriate mirror planes.

IV. DISCUSSION AND CONCLUSIONS

In general, for each surface of $\{n\ n\ m\}$ family only one mirror plane of {110} type can be found. This leads to only one pair of protected Dirac points, which correspond to the two L points situated at this mirror plane in the 3DBZ. Two special cases can be distinguished: $n = m = 1$ and $n = 0$. While for the former case three {110} mirror planes exist, for the latter case there are two such planes (compare Fig. 1). We note that despite the different number of mirror planes, the number of Dirac points should be the same for the {001} and {111} surfaces, because for the latter one L point is common for all three mirror planes. Therefore, in both these cases four Dirac points should appear in the band structure. In both these cases all L points are located at the symmetry planes and the corresponding Dirac points should be topologically protected.

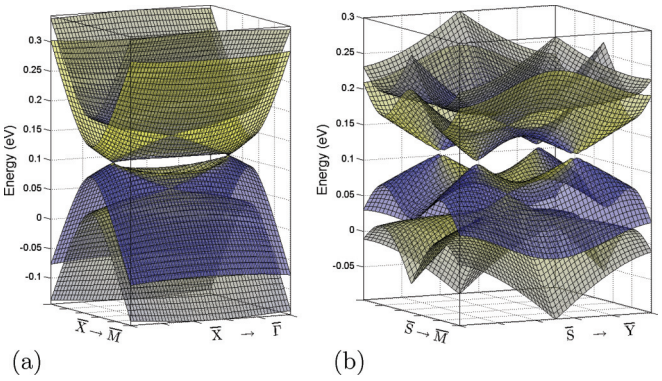

FIG. 6. (Color online) The three-dimensional view of the band structure in the vicinity of the $\overline{X}$ point for the (001)-oriented surface (a) and in the vicinity of the $\overline{S}$ point of the 2DBZ for the (110)-oriented surface (b) of $Pb_{0.4}Sn_{0.6}Te$.

As shown in the Appendix, for any $\{n\ k\ m\}$ surface type the four L points in the 3DBZ project to four different points of the 2DBZ only when all n, k, and m surface indices have the same parity. Otherwise they project in pairs. Thus, when the parities of n and m in $\{n\ n\ m\}$ surfaces are different, the L points are projected in pairs. In general, only one pair of Dirac points is guaranteed to appear on the mirror symmetry line in the vicinity of the projection of one L-point pair and is topologically protected. However, for the special case of {001} surface type there are two mirror symmetry lines and all four Dirac points are topologically protected. Two of them are shown in Fig. 6(a). Similar band structure is obtained for the (110) surface in the vicinity of the $\overline{Y}$ point of the 2DBZ. In this case only one pair of Dirac points exists—for the L points projected to $\overline{S}$ instead of Dirac points gaps occur for the (110) surface states, as shown in Fig. 6(b).

In the $\{n\ n\ m\}$ case the L points project to different points in the 2DBZ only when n and m have the same parity (this means of course that they are both odd numbers).

In Fig. 7 the band structures around the $\overline{\Gamma}$ and $\overline{M}$ points obtained for the (111)-oriented cation surface are presented [analogous results are obtained for the (111)-oriented slab with

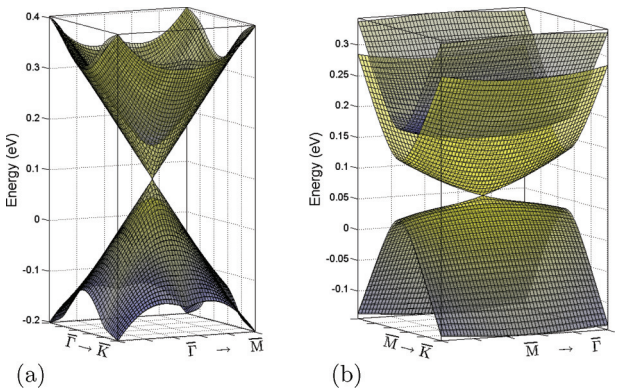

FIG. 7. (Color online) The three-dimensional view of the band structure in the vicinity of the $\overline{\Gamma}$ (a) and $\overline{M}$ (b) points of the 2DBZ for the (111)-oriented cation surface of $Pb_{0.4}Sn_{0.6}Te$.

anions at the surface]. While at the $\overline{\Gamma}$ point an isotropic Dirac cone is observed, the band structure around $\overline{M}$ is strongly anisotropic, i.e., along the $\overline{M}$-$\overline{\Gamma}$ line it depends differently on the k values than in $\overline{M}$-$\overline{K}$ direction. The difference in shape of the band structures is due to different orientations of the constant-energy ellipsoids around different L points. While the L_1 ellipsoid is projected along its long axis, the ellipsoids for the other three L points are tilted to the projection direction.

Finally, the chiral spin texture of the surface states of $Pb_{0.4}Sn_{0.6}Te$ for all considered surfaces (001), (110), and (111) has been obtained. While our calculations show a "multivortical" spin structure for the (001) and (110) surface states, for the (111) anion and cation surfaces a "single-vortical" spin texture is anticipated. As revealed by our studies, spin polarization seems to be inherent to all (001), (110), and (111) surface states in narrow-gap IV-VI semiconductors in their TCI phase. We note that in the cases of (001) and (110) surfaces the topology of the constant-energy lines undergoes a Lifshitz transition (compare Fig. 5), similar to that predicted and observed for SnTe.[12,13] It seems that such a transition has been also observed in $Pb_{1-x}Sn_xTe$.[15] It should be noted that in the calculations presented here neither the surface reconstruction nor the phenomena related to the polarity of the (111) surfaces has been taken into account. Although these effects can lead to some modification of the surface energy spectrum, the conclusions presented here are determined by the topological properties of the bulk electronic band structure of the material.

We expect qualitatively similar effects to those described above to occur also for the states of the (001)-, (110)-, and (111)-oriented interfaces between a TCI and a normal insulator. For the (111) interface, for example, this has already been shown in Ref. 10. However, all the experiments for the TCI phase in PbTe-SnTe solid solutions have been performed on (001) surfaces, because, as is well known, the (001) surfaces are the cleavage planes in the $Pb_{1-x}Sn_xTe$ material. Still, it is also well known that using the BaF_2 substrate allows the growth of Se- and Te-based rocksalt IV-VI compound crystals and heterostructures in the [111] direction and that (111)-oriented IV-VI structures have the highest mobilities and electron mean free paths.[23] These make the (111) surface states most interesting for the study of TCIs and other transport phenomena. We note that in the case of the interfaces the reconstruction and the polarity phenomena related to the change of stoichiometry do not appear. Instead, due to the different lattice parameters of the heterostructure constituents, strain can play a role in the energy states of the interface. Still, the overall energy structure of the interface states shows the same features as for the corresponding surface states.[10] It should also be noted that for the (111)-oriented interface there is only one Dirac cone at each L-point projection, in contrast to the two separate Dirac cones for the cation- or anion-terminated (111) surfaces.

It was also shown that using the GaAs substrate with a thick CdTe buffer allows growth by molecular-beam epitaxy of good-quality PbTe-based structures.[24] As (110)-oriented GaAs substrates are available, it seems that by the same method the growth of IV-VI structures along the [110] crystallographic axis should also be possible. We are convinced that our study of the surface states for $Pb_{1-x}Sn_xTe$ TCI crystals oriented in these directions can be very useful for predicting or describing various phenomena in such structures.

ACKNOWLEDGMENTS

We would like to thank Tomasz Story and Marta Galicka for their diverse support. Financial support from the EC Network SemiSpinNet (Grant No. PITN-GA-2008-215368), the European Regional Development Fund through an Innovative Economy Grant (No. POIG.01.01.02-00-108/09), and the Polish National Science Centre (NCN) Grant No. 2011/03/B/ST3/02659 is gratefully acknowledged.

APPENDIX: RULES FOR THE L-POINT PROJECTION ONTO AN ARBITRARY SURFACE

The study of the L-point projection onto an arbitrary surface is motivated by the results presented above that in the case of (001) and (110) surfaces two pairs of nonequivalent L points are projected onto two nonequivalent points in the 2DBZ, whereas for the (111) surface four L points are projected onto four nonequivalent points in the appropriate 2DBZ. Therefore, we would like to find a general rule to describe for which surfaces L points are projected separately and for which they are projected in pairs. Let us first define the vectors $\vec{L}_i$ for the four nonequivalent L points in the first Brillouin zone as $\vec{L}_i = \vec{G}_i/2$, $i = 1,\ldots,4$, where $\vec{G}_i$, in units of $2\pi/a_0$, are given by

$$\vec{G}_1 = \begin{pmatrix} 1 \\ 1 \\ 1 \end{pmatrix}, \quad \vec{G}_2 = \begin{pmatrix} 1 \\ 1 \\ -1 \end{pmatrix},$$

$$\vec{G}_3 = \begin{pmatrix} 1 \\ -1 \\ -1 \end{pmatrix}, \quad \vec{G}_4 = \begin{pmatrix} 1 \\ -1 \\ 1 \end{pmatrix}. \tag{A1}$$

The first three $\vec{G}_i$ vectors we choose as a basis in reciprocal space.

One can say that two points L_i and L_j project onto the same point in the 2DBZ when L_i and L_j (or any other point equivalent to L_j) are located on the same line along the projection direction. For a given $(s_1\ s_2\ s_3)$ surface the projection direction is given by the vector $\vec{S} = (s_1\ s_2\ s_3)^T$. Thus, the two L points project onto the same point of the 2DBZ when

$$\vec{L}_i - \vec{L}_j = \vec{G} + \alpha\vec{S}, \tag{A2}$$

where $\vec{G}$ is the reciprocal net vector $n_1\vec{G}_1 + n_2\vec{G}_2 + n_3\vec{G}_3$ and n_1,n_2,n_3 are integer numbers. The condition for the s_1,s_2,s_3 surface indices leading to the projection of L_i and L_j points onto the common point in the 2DBZ will be

$$\vec{L}_i - \vec{L}_j = \begin{pmatrix} l_1 \\ l_2 \\ l_3 \end{pmatrix} = \begin{pmatrix} n_1+n_2+n_3 \\ n_1+n_2-n_3 \\ n_1-n_2-n_3 \end{pmatrix} + \alpha \begin{pmatrix} s_1 \\ s_2 \\ s_3 \end{pmatrix}. \tag{A3}$$

We note that s_1,s_2,s_3, being the surface indices, are relative primes. Moreover, l_1,l_2,l_3 are either ±1 or 0 and the l_k components for any L_i,L_j pair have different parities—at least one l_k is equal to 0 and at least one has to be ±1. In contrast, for any set of n_k $(k = 1,\ldots,3)$ all three components of $\vec{G}$ have

the same parity. We observe that Eq. (A3) can be satisfied only when two conditions are simultaneously fulfilled: (a) α is an odd integer (one can always find a solution with $\alpha = 1$) and (b) the parities of s_k are either the same as the parities of the corresponding l_k (with even $\vec{G}$ components) or s_k and l_k have opposite parities (with odd $\vec{G}$ components). Thus, we can conclude that two L points project to the same point on the 2DBZ of an (s_1,s_2,s_3) surface only when the parities of the s_k indices are various.

Let us take, for example, two pairs of L points, (L_1,L_2) and (L_4,L_3). For both $\vec{L}_1 - \vec{L}_2$ and $\vec{L}_4 - \vec{L}_3$, $l_1 = l_2 = 0$ and $l_3 = 1$. This means that the condition (A2) can be satisfied with the same surface indices for these two pairs—in this particular case the parity of the s_3 index has to be opposite to the parity of s_1 and s_2. We note that these indices do not satisfy the condition (A2) for the (L_1,L_3) pair. Thus, the two (L_1,L_2) and (L_3,L_4) pairs are projected onto two different, nonequivalent points in the 2DBZ.

After examination of all possible L-point pairs we can conclude that the following four nonequivalent L points are projected in two pairs on an (s_1,s_2,s_3) surface:

(L_1,L_2) and (L_3,L_4), if the s_3 parity is opposite to the s_1 and s_2 parities;

(L_1,L_3) and (L_2,L_4), if the s_1 parity is opposite to the s_2 and s_3 parities;

(L_1,L_4) and (L_2,L_3), if the s_2 parity is opposite to the s_1 and s_3 parities.

In contrast, when the surface indices s_1,s_2,s_3 have the same parity (they are odd numbers, as the indices are relative primes), the condition (A2) cannot be satisfied for any pair of L points. Then the four L points are projected onto four separate nonequivalent points in the 2DBZ. Moreover, one can prove by similar considerations that in this case one of the L points has to be projected onto the $\overline{\Gamma}$ point, in contrast to the other L points, which are projected onto the edges of the 2DBZ.

*buczko@ifpan.edu.pl

[1] M. Z. Hasan and C. L. Kane, Rev. Mod. Phys. **82**, 3045 (2010).

[2] X.-L. Qi and S.-C. Zhang, Rev. Mod. Phys. **83**, 1057 (2011).

[3] C. L. Kane and E. J. Mele, Phys. Rev. Lett. **95**, 146802 (2005).

[4] L. Fu and C. L. Kane, Phys. Rev. B **76**, 045302 (2007).

[5] L. Fu, C. L. Kane, and E. J. Mele, Phys. Rev. Lett. **98**, 106803 (2007).

[6] M. König, S. Wiedmann, C. Brüne, A. Roth, H. Buhmann, L. W. Molenkamp, X.-L. Qi, and S.-C. Zhang, Science **318**, 766 (2007).

[7] D. Hsieh, D. Qian, L. Wray, Y. Xia, Y. S. Hor, R. J. Cava, and M. Z. Hasan, Nature (London) **452**, 970 (2008).

[8] D. Hsieh, Y. Xia, D. Qian, L. Wray, J. H. Dil, F. Meier, J. Osterwalder, L. Patthey, J. G. Checkelsky, N. P. Ong, A. V. Fedorov, H. Lin, A. Bansil, D. Grauer, Y. S. Hor, R. J. Cava, and M. Z. Hasan, Nature (London) **460**, 1101 (2009).

[9] I. Knez, R.-R. Du, and G. Sullivan, Phys. Rev. Lett. **107**, 136603 (2011).

[10] R. Buczko and L. Cywinski, Phys. Rev. B **85**, 205319 (2012).

[11] L. Fu, Phys. Rev. Lett. **106**, 106802 (2011).

[12] T. H. Hsieh, H. Lin, J. Liu, W. Duan, A. Bansil, and L. Fu, Nat. Commun. **3**, 982 (2012).

[13] Y. Tanaka, Z. Ren, T. Sato, K. Nakayama, S. Souma, T. Takahashi, K. Segawa, and Y. Ando, Nat. Phys. **8**, 800 (2012).

[14] P. Dziawa, B. J. Kowalski, K. Dybko, R. Buczko, A. Szczerbakow, M. Szot, E. Łusakowska, T. Balasubramanian, B. M. Wojek, M. H. Berntsen, O. Tjernberg, and T. Story, Nat. Mater. **11**, 1023 (2012).

[15] S.-Y. Xu, C. Liu, N. Alidoust, M. Neupane, D. Qian, I. Belopolski, J. D. Denlinger, Y. J. Wang, H. Lin, L. A. Wray, G. Landolt, B. Slomski, J. H. Dil, A. Marcinkova, E. Morosan, Q. Gibson, R. Sankar, F. C. Chou, R. J. Cava, A. Bansil, and M. Z. Hasan, Nat. Commun. **3**, 1192 (2012).

[16] L. Fu and C. L. Kane, Phys. Rev. Lett. **109**, 246605 (2012).

[17] B. M. Wojek, R. Buczko, S. Safaei, P. Dziawa, B. J. Kowalski, M. H. Berntsen, T. Balasubramanian, M. Leandersson, A. Szczerbakow, P. Kacman, T. Story, and O. Tjernberg, Phys. Rev. B **87**, 115106 (2013).

[18] J. Liu, W. Duan, and L. Fu, arXiv:1304.0430.

[19] Y. J. Wang, W.-F. Tsai, H. Lin, S.-Y. Xu, M. Neupane, M. Z. Hasan, and A. Bansil, Phys. Rev. B **87**, 235317 (2013).

[20] C. S. Lent, M. A. Bowen, J. D. Dow, R. S. Allgaier, O. F. Sankey, and E. S. Ho, Superlattices Microstruct. **2**, 491 (1986).

[21] M. S. Bahramy, P. King, A. de la Torre, J. Chang, M. Shi, L. Patthey, G. Balakrishnan, P. Hofmann, R. Arita, N. Nagaosa, and F. Baumberger, Nat. Commun. **3**, 1159 (2012).

[22] F. Zhang, C. L. Kane, and E. J. Mele, Phys. Rev. B **86**, 081303 (2012).

[23] G. Grabecki, K. A. Kolwas, J. Wrobel, K. Kapcia, R. Puzniak, R. Jakiela, M. Aleszkiewicz, T. Dietl, G. Springholz, and G. Bauer, J. Appl. Phys. **108**, 053714 (2010).

[24] M. Szot, K. Dybko, P. Dziawa, L. Kowalczyk, E. Smajek, V. Domukhovski, B. Taliashvili, P. Dluzewski, A. Reszka, B. J. Kowalski, M. Wiater, T. Wojtowicz, and T. Story, Cryst. Growth Des. **11**, 4794 (2011).